A High Power Density Intermediate-Temperature Solid Oxide Fuel Cell with Thin $(La_{0.9}Sr_{0.1})_{0.98}(Ga_{0.8}Mg_{0.2})O_{3-\delta}$ Electrolyte and Nano-Scale Anode

Zhan Gao, Elizabeth C. Miller, and Scott A. Barnett*

Solid oxide fuel cells (SOFCs) with thin $(La_{0.9}Sr_{0.1})_{0.98}Ga_{0.8}Mg_{0.2}O_{3-\delta}$ (LSGM) electrolytes are primary candidates for achieving high (> 1 W cm^{-2}) power density at intermediate (< 650 °C) temperatures. Although high power density LSGM-electrolyte SOFCs have been reported, it is still necessary to develop a fabrication process suitable for large-scale manufacturing and to minimize the amount of LSGM used. Here we show that SOFCs made with a novel processing method and a $Sr_{0.8}La_{0.2}TiO_{3-\alpha}$ (SLT) oxide support can achieve high power density at intermediate temperature. The SLT support is advantageous, especially compared to LSGM supports, because of its low materials cost, electronic conductivity, and good mechanical strength. The novel process is to first co-fire the ceramic layers – porous SLT support, porous LSGM layer, and dense LSGM layer – followed by infiltration of nano-scale Ni into the porous layers. Low polarization resistance of 0.188 Ωcm^2 was achieved at 650 °C for a cell with an optimized anode functional layer (AFL) and an (La,Sr)(Fe,Co)O_3 cathode. Maximum power density reached 1.12 W cm^{-2} at 650 °C, limited primarily by cathode polarization and ohmic resistances, so there is considerable potential to further improve the power density.

1. Introduction

Most solid oxide fuel cells (SOFCs) operate at 750–900 °C, providing the advantages of high efficiency, high power density, and elimination of expensive precious-metal electro-catalyst materials. However, the high operating temperature also introduces difficult challenges related to high materials cost, issues with seals and interconnects, startup time, and long-term durability. Development of high-performance intermediate-temperature (≤650 °C) SOFCs (IT-SOFCs) can mitigate the above problems, but the challenge is to retain the high power density without the use of expensive catalysts. Thus, many studies have been reported aiming at developing IT-SOFC component materials characterized by low area specific resistance at intermediate temperature.[1]

A key challenge in IT-SOFCs is to achieve a low resistance electrolyte, which usually requires a thin (<10 μm) electrode-supported layer of a fast oxygen ion conducting material. Strontium- and magnesium-doped lanthanum gallate (LSGM) is a candidate electrolyte material due to its high oxygen ion conductivity (0.03 S cm^{-1} at 600 °C,[2] comparable to doped ceria but without the electronic conductivity that compromises cell open-circuit voltage. However, it is difficult to manufacture SOFCs with thin LSGM electrolytes on conventional Ni-based anode supports, because of Ni-LSGM reactions and La loss from LSGM during high-temperature co-firing.[3] Thus, thin-LSGM SOFCs have often been produced using pulsed-laser deposition, where temperatures are low enough to avoid the above problems.[4] However, pulsed-laser deposition is not considered suitable for large-scale manufacturing.

An alternate processing scheme was recently reported that avoids the above difficulties—co-firing a porous LSGM support with a thin dense LSGM layer, and then infiltrating Ni to form the anode at lower temperature.[5] Infiltrating Ni after high temperature processing minimizes deleterious LSGM-Ni reactions while producing nano-scale Ni particles with very high three-phase boundary density.[6] However, the high cost of Ga is problematic in these cells, because of the thick (≈500 μm) LSGM support. Other issues with an LSGM anode support include its relatively low mechanical strength, e.g. average strength is only 55 ± 11 MPa at 900 °C for $La_{0.9}Sr_{0.1}Ga_{0.8}Mg_{0.2}O_{3-\delta}$ samples with density higher than 98.5%,[7] and lack of electronic conductivity, e.g. the lower boundary of electrolytic domain (defined as the ionic transference number t_{ion}≥0.99) for $La_{0.9}Sr_{0.1}Ga_{0.8}Mg_{0.2}O_{3-\delta}$ is 10^{-23} atm at 1000 °C,[8] such that it does not contribute to current collection. We recently demonstrated SOFCs where the porous $(La_{0.9}Sr_{0.1})_{0.98}Ga_{0.8}Mg_{0.2}O_{3-\delta}$ (LSGM) support is replaced with $Sr_{0.8}La_{0.2}TiO_{3-\alpha}$ (SLT), but the power density was relatively low, 430 mW cm^{-2} at 650°C.[9]

Here we demonstrate, for the first time, thin-LSGM-electrolyte SOFCs on SLT supports yielding high power densities at temperatures ≤ 650 °C. SLT supports have substantial advantages compared to LSGM including low material cost,[10] and the LSGM electrolyte and anode functional layer (AFL) in these cells are < 50 μm thick, electronic conductivity (4 Scm^{-1} at 800 °C in humidified hydrogen for the sample initially fired in

Dr. Z. Gao, E. C. Miller, Prof. S. A. Barnett
Department of Materials Science and Engineering
Northwestern University
2220 Campus Drive
Evanston, IL, 60208 United States of America
E-mail: zhan.gao@northwestern.edu

DOI: 10.1002/adfm.201400295

air[11]), and good mechanical strength (a strength of 75 MPa by four point bend testing for the SLT with porosity of 40%).[11] SLT contains enough La to avoid La loss from LSGM, has a similar average thermal expansion coefficient as LSGM, exhibits excellent overall stability, and was previously shown to have substantial advantages as the support in thin-YSZ-electrolyte cells.[12,13] SLT is also stable during redox cycling, resistant to coking, and unaffected by sulfur impurities.[13] A key reason for the good power density in the present cells is the improved infiltrated Ni-LSGM anode functional layer (AFL), which exhibits low polarization resistance due to a high density of Ni-LSGM three phase boundaries (TPBs).

2. Results

2.1. Microstructural Evaluation

Figure 1 shows low-magnification scanning electron microscopy (SEM) overview images of the cells with different anode functional layers (AFLs) and 15.0 vol.% Ni, taken after electrochemical testing. The thicknesses of the anode functional layers are about 30 μm, and the SLT support is about 500 μm thick. The 10 wt.%, 20 wt.%, 30 wt.% and 40 wt.% weight percent of PMMA pore formers gives the AFL porosity of ~15%, 22%, 26% and 33%, respectively. The average pore sizes formed by the pore formers were about 2 μm. The porosity and surface area of the AFLs appear to increase with increasing PMMA amount. Figure 1d presents the SEM energy-dispersive spectroscopy line scans for the cell (Figure 1b). Both La and Sr intensities agreed qualitatively with the compositions of each layer, with no evidence of re-distribution. This indicates that the La content in SLT was sufficient to prevent significant loss of La from LSGM, which has proved to be problematic previously when LSGM was cofired with other materials.[3,14] The Ti intensity was highest in the SLT support and the apparent Ti intensity in the LSGM electrolyte and AFL was the artifact with slight intensity from nearby La and O peaks,[9] since our previous research has found that Ti intensity in LSGM electrolyte layer was less than 1 at.%, the detection limit of EDS, even after co-firing at 1400 °C with SLT in direct contact with the LSGM.[9] The Ni signal was only present in the SLT support and LSGM AFL while the apparent Ni intensity in the LSCF-GDC cathode was found to be the artifact of peak overlap with La, Co, Gd and Ce.[9]

Figure 2 presents higher-magnification SEM images of the AFLs in cells with 30 wt.% weight percent of PMMA and different Ni loading amounts. As shown in Figure 2(a), the internal pore surfaces of the AFL are covered by Ni particles with an average particle diameter of ≈100 nm. However, it appears that many of the Ni particles are not in contact with each other, such that these particles are electrically isolated and hence electrochemically inactive. As the Ni loading increases (Figures 2(b) and 2(c)), there is a higher density of Ni particles in the LSGM pores, and they appear to be much better connected. The Ni particles in the pores of the SLT support (not shown) also connect better at higher loading, which should help improve the support electronic conductivity. In general, the high LSGM internal surface area and small size of the Ni particles in these

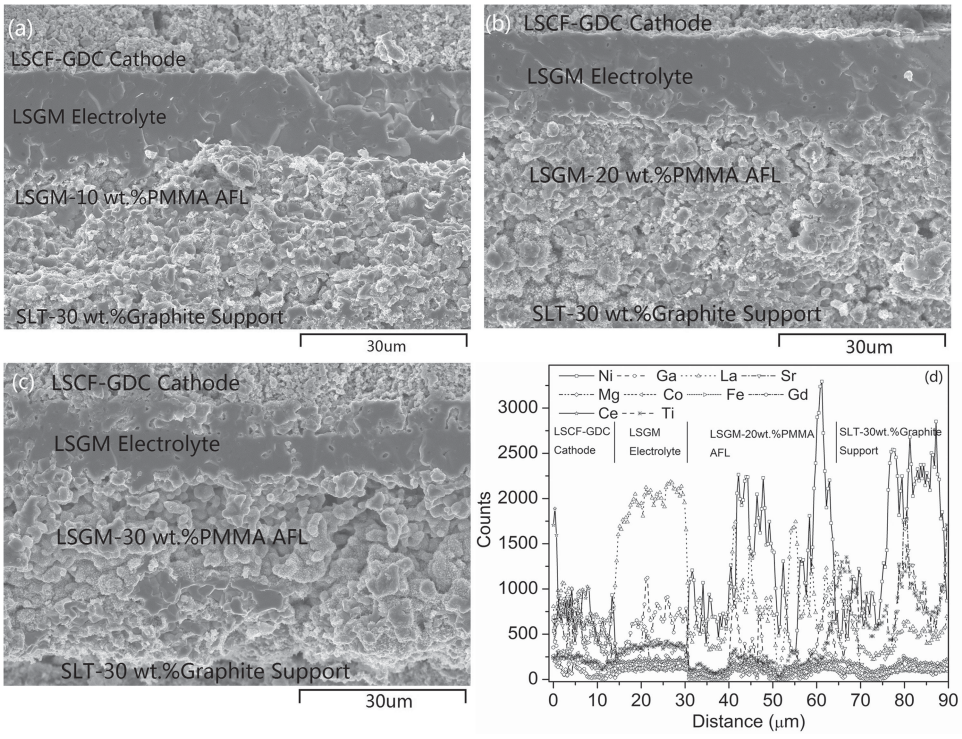

Figure 1. Cross-sectional SEM images for the cells with different PMMA weight percentages in the anode functional layers: a) 10 wt.%, b) 20 wt.%, c) 30 wt.%. All AFLs contained 15.0 vol.% Ni; d) The intensity line scan from Ni, Ga, La, Sr, Mg, Co, Fe, Gd, Ce and Ti signals for the (b) cell with PMMA weight percent of 20 wt.% and 15.0 vol.% Ni in the AFL.

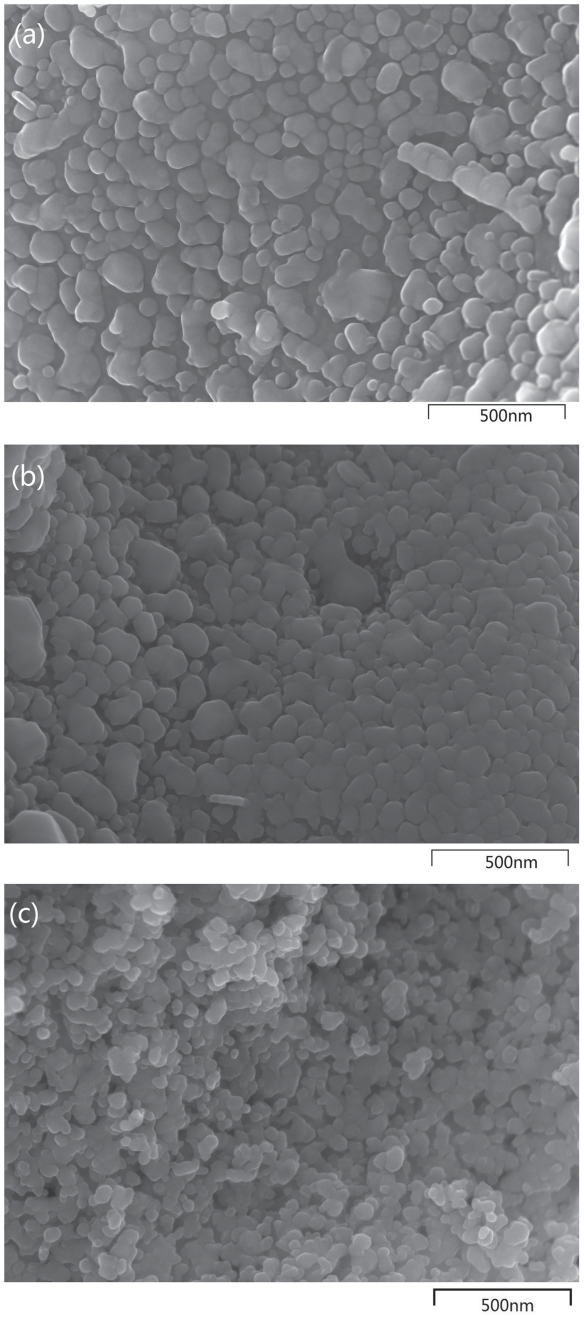

Figure 2. SEM images of AFLs with PMMA weight percentage of 30 wt.% and different Ni loading amounts of a) 6.7 vol.% Ni, b) 10.8 vol.% Ni and c) 15.0 vol.% Ni.

AFLs provides high three phase boundary (TPB) density. As discussed previously for LSGM-supported cells,[5,15,16] this facilitates the H_2 oxidation reactions on the anode.

Figure 3 shows the XRD patterns of SLT and LSGM powders, which both show peaks indicating perovskite structure with no evidence of secondary phases. For the mixture of SLT and LSGM fired together at 1400 °C, no additional peaks were detected, indicating that there were no secondary phases formed via reactions between SLT and LSGM, within a detection limit of a few atomic percent. The SLT and LSGM peaks

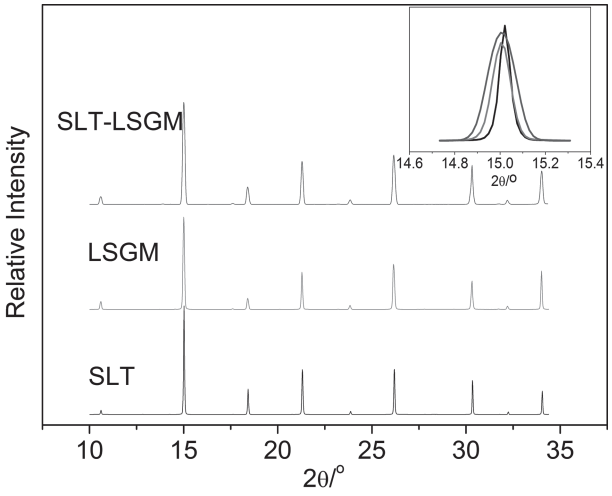

Figure 3. Synchrotron-based XRD patterns comparing SLT, LSGM, and SLT-LSGM mixed powders after firing at 1400 °C. The insert shows a magnified view of the main peaks at $2\theta \approx 15°$

are overlapped, since they have similar size cations, as shown in the insert figure. Overall, these results indicate that SLT and LSGM are quite compatible.

2.2. Current-Voltage Characteristics

This section presents results on various SOFCs with differently processed Ni-LSGM AFLs. **Figure 4** presents the characteristics of a SOFC that was typical of those prepared using optimized AFL processing conditions. Current voltage data showed positive curvature at lower operating temperatures, indicative of activation polarization. There was also evidence of a current limitation at 3.5 A cm^{-2}, which can be due to the mass transport limitation, mostly likely diffusion of H_2 in the thick SLT support.[11,13] Open circuit voltages (OCVs) decreased with increasing temperature, e.g., from 1.086 V at 450 °C to 1.052 V at 650 °C. The OCVs are lower than the theoretical value, e.g., 1.13 V at 600 °C, since the present cell test configuration, utilizing Ag seals around the edges of the anode support, typically results in a small gas leakage.[17] Maximum power density values increased with increasing temperature, e.g., from 0.22 W cm^{-2} at 500 °C to 1.12 W cm^{-2} at 650 °C. The 100 h stability test under 0.4 A cm^{-2} at 600 °C shows a decrease in cell voltage of at most a few percent, which may be due to Ni coarsening, as reported for Ni infiltrated YSZ anodes.[18]

Figure 5 shows the variation of the maximum power density, measured at different operating temperatures, with different AFLs at a constant Ni loading of 15.0 vol.%. Note that the cell OCV value, cathode resistance, and ohmic resistance did not vary much from cell to cell, so the maximum power density provides a good measure of how the AFL affects cell performance. Power density values increased continuously with increasing porosity in AFL. Values for the cell with 40 wt.% PMMA in the AFL (porosity of 33%) are not shown in Figure 5, because pores >10 μm in size were present in the AFL, leading to a poor quality LSGM electrolyte. As a result, this cell had low

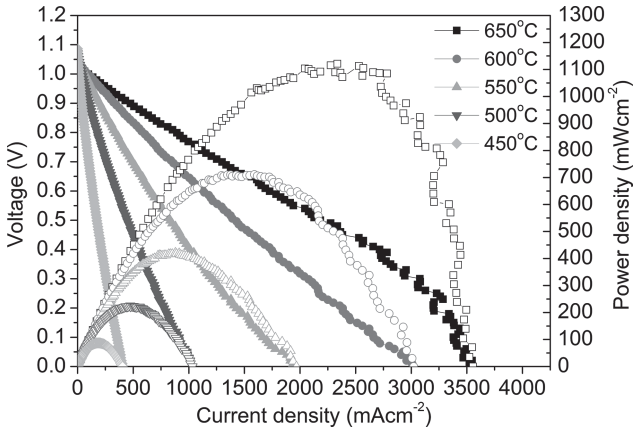

Figure 4. Voltage and power density versus current density measured in air and 50 sccm humidified H_2 at different temperatures, for the fuel cell with AFL porosity of 26% and 15.0 vol.% Ni in AFL. Scatter in the data at high current density were due to the use of stagnant air at the cathode.

open circuit voltage and maximum power density (0.96 V and 0.80 W cm^{-2} at 650 °C), and was not directly comparable with the others in Figure 5. **Figure 6** shows the variation of the maximum power density, measured at different operating temperatures, with the Ni loading for an AFL porosity of 26%. Power density increased substantially when the Ni loading increased from 4.3 to 6.7 vol.%, but further increases in Ni loading up to 15.0 vol.% yielded only minor further improvement.

2.3. Electrochemical Impedance Spectroscopy (EIS)

EIS was measured with cells at OCV in order to separate the contributions from ohmic, cathodic and anodic parts of the cell resistance. **Figure 7** shows the spectra for cells with different porosity in the AFLs, and **Figure 8** shows the results for cells with different Ni loading amounts. In general, the ohmic resistance and the total electrode polarization resistance decreased with increasing porosity and increasing Ni loading in the AFL. The decrease in ohmic resistance from 4.3 to 6.7 vol.% Ni was

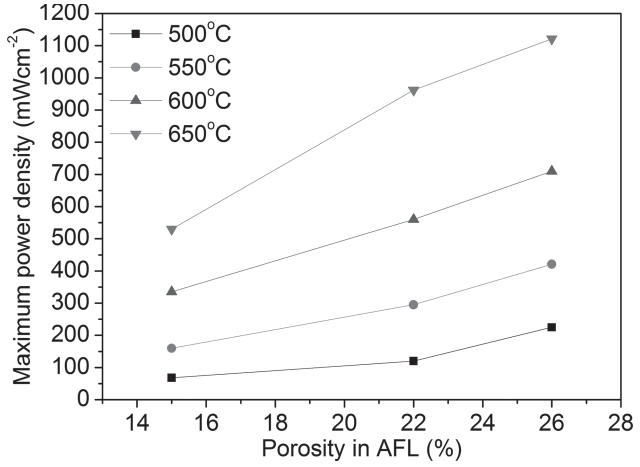

Figure 5. Maximum power density measured at different temperatures for cells with different AFL porosities, for a fixed Ni content of 15.0 vol.%.

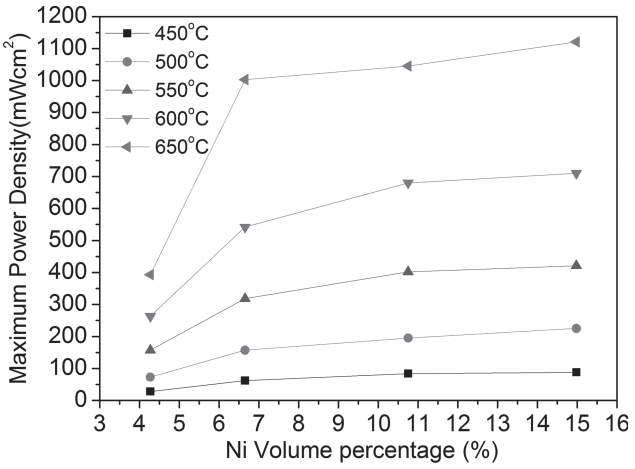

Figure 6. Maximum power density measured at different temperatures for cells with different Ni loading amounts.

especially marked. Three different responses can be clearly distinguished in all of the spectra. The EIS data in Figures 7 and 8 were fitted using an equivalent circuit with three or four Cole elements in series with an inductor and resistor. This model provided a more accurate measure of ohmic resistance than the high-frequency real-axis intercept, which was shifted due to inductances in the measurement apparatus. While the equivalent circuit model provided reasonable fits, it was not possible with the present data to determine the physical processes associated with the Cole elements. Prior results on similar cells[9] showed that all three responses varied with hydrogen partial pressure, indicating that they were anode processes, but prior data on these LSCF-GDC cathodes show responses peaking at 100–1000 Hz,[19] overlapped with the anode responses. Thus, the results below focus on the total electrode polarization resistance; since the cathodes in all cells were nominally identical, changes in the total resistance can be ascribed to changes in the anodes.

Figure 9 summarizes the EIS fitting results, showing the cell ohmic, electrode polarization, and total cell resistances at 650 °C versus different porosities (a) and Ni loading amounts (b) in AFL. As shown in Figure 9a, the ohmic resistance decreased with increasing porosity from 0.15 Ω cm^2 to 0.067 Ω cm^2. The lowest electrode resistance of ≈0.188 Ω cm^2 was achieved for the AFL with porosity of 26%. The total cell resistance, i.e., the sum of the ohmic and electrode parts, had its lowest value at 0.26 Ω cm^2 for the AFL with porosity of 26% and 15.0 vol.% Ni. Figure 9b shows a substantial decrease in total cell resistance with increasing Ni loading, consistent with the increases in power density noted earlier. The ohmic resistance decreases with Ni loading; the major decrease on increasing the loading to 6.7 vol.% Ni, noted earlier, is clear. The electrode resistance decreases slightly with increasing Ni loading. The lone exception was for 10.8 vol.% Ni loading, probably due to the cell-to-cell variations.

3. Discussion

A comparison of the present cells to LSGM supported cells with the same cathode[5] shows that maximum power densities were

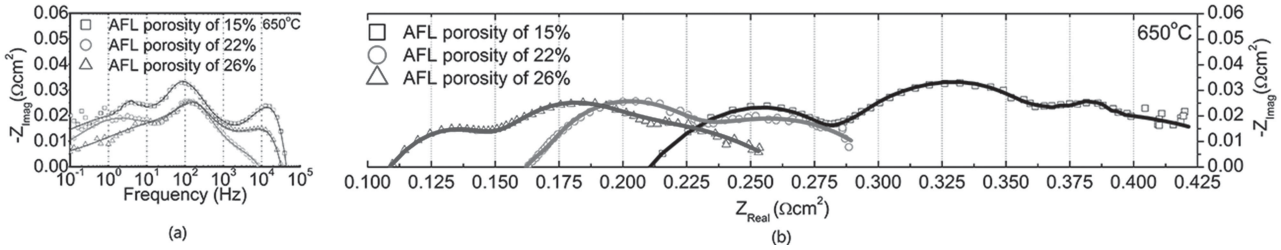

Figure 7. a) Bode and b) Nyquist plots of impedance data taken at 650 °C for SOFCs fabricated with different AFL porosities, for a fixed Ni loading of 15.0 vol%. The data points are the measured data and the solid lines are the fitting results.

similar, although the present cells yielded slightly lower power at operating temperatures ≥600 °C and slightly higher power at ≤550 °C. However, ≈90% of the LSGM has been replaced by SLT in the present cells, which should substantially decrease the materials cost. However, utilizing LSGM instead of SLT in the AFL scaffold is important for yielding high power density,[9] because of the much better oxygen ion conductivity of LSGM compared to SLT. The ohmic resistance for the present optimized cell is 0.067 Ω cm^2 at 650 °C, smaller than the LSGM supported cell, 0.098 Ω cm^2 at 650 °C,[20] although the electrolyte thicknesses were similar. This decrease might be explained by improved current collection due to the electronic conductivity of SLT, whereas LSGM is a pure ionic conductor. Overall IT-SOFC performance can presumably be improved further by reducing the LSGM electrolyte thickness and via an improved cathode.[15,21]

An important aspect of the good cell performance was the optimization of the infiltrated Ni in the AFL. The present decrease in ohmic and polarization resistance with increasing Ni loading (Figure 9b) is similar to prior reports for Ni-infiltrated LSGM AFLs,[5] where it was concluded that the high ohmic resistance was due to insufficient electronic current pathways in the infiltrated Ni at low loadings. The ohmic resistance decreased substantially on going from 4.3 vol.% to 6.7 vol.% Ni, but increased less rapidly for further Ni loading increases. This decrease is as expected, because the ohmic resistance should tend to saturate as the Ni becomes more fully percolated (10.8 vol.% Ni). For low Ni loading, a substantial part of the AFL furthest from the SLT may be electrically isolated from the current collector. This portion of the AFL can thus only conduct ionically in the LSGM phase, such that it becomes like an additional thickness of LSGM electrolyte, increasing the ohmic resistance. In addition, the electronic conductivity of SLT is not very high, such that there is an ohmic resistance contribution from the support;[13] thus, increasing the Ni loading should reduce this resistance contribution. On the other hand, there is only a minor decrease in polarization resistance with increasing Ni loading. This observation can be explained by a trade-off between increased Ni percolation and an increase in Ni particle size (and hence reduced TPB density).[5]

Compared with the traditional Ni-cermet anode (≈30 vol.% Ni,[22] the percolation threshold of the infiltrated anode was much lower (10.8 vol.% Ni), but was consistent with previous results for infiltrated Ni-YSZ anodes.[23] An advantage of this relatively low Ni content, where the Ni forms a network on the surface of the electrode rather than a composite with the electrode material at low firing temperatures, is that dimensional changes of the anode during redox cycles are not expected to cause anode damage.[24]

Higher cell ohmic and polarization resistance were observed for low AFL porosity. A similar phenomenon was reported previously for SLT-supported LSGM cells,[9] and was explained by noting that there was probably a substantial fraction of closed pores, or pores where little Ni penetrated. In this case, only Ni near the SLT current collector has electrical connection to the external circuit, and most of the LSGM anode functional layer acts as part of the electrolyte, yielding the increased ohmic and polarization resistances. More pores were created in the AFLs by increasing the PMMA weight percent, which increases the pore percolation[25] and the internal surface area of the anode functional layer. The AFL with 30 wt% PMMA pore former (porosity of ≈26%) was optimal, and this should be well above the percolation threshold. Further increase in AFL porosity did not lead to further improvements in AFL resistance, due to the formation of very large pores. In summary, the optimized porous and percolated

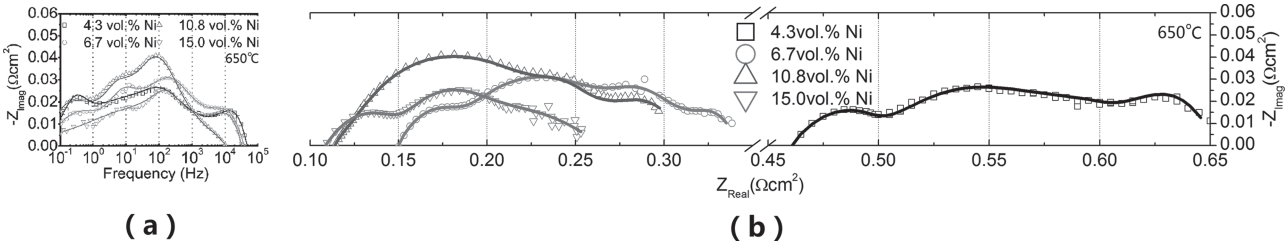

Figure 8. a) Bode and b) Nyquist plots of impedance data taken at 650 °C for cells with different Ni loadings, for a fixed AFL porosity of 26%. The data points are the measured data and the solid lines are the fitting results.

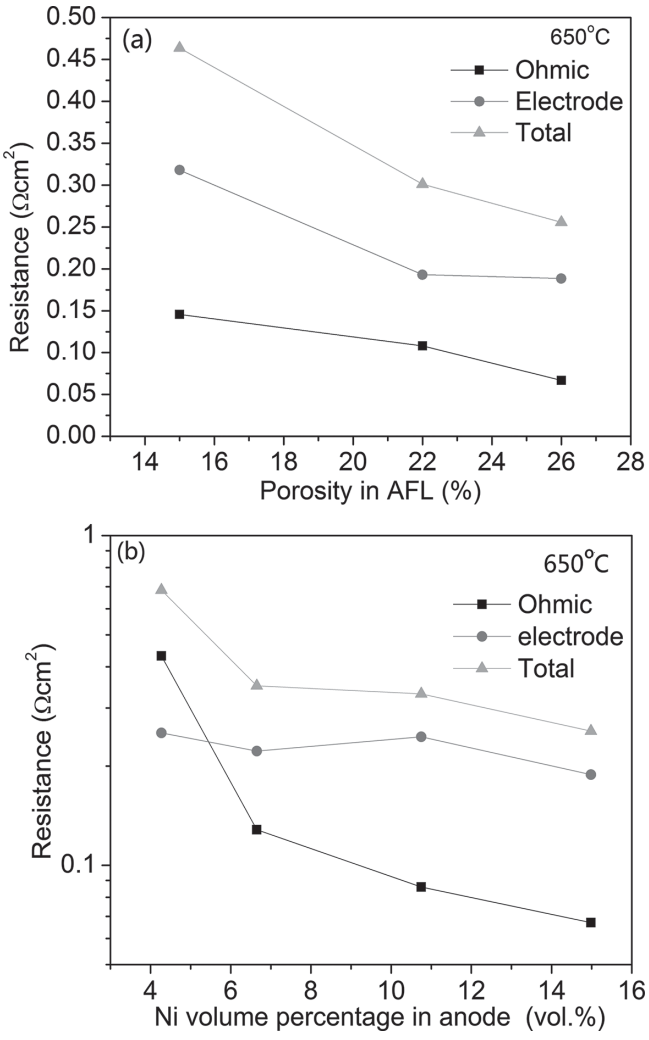

Figure 9. Ohmic resistance, electrode polarization resistance, and total resistance versus a) AFL porosity at a Ni loading of 15.0 vol.% and b) Ni loading volume percentage at an AFL porosity of 26%.

LSGM scaffold provides both high oxygen ionic conductivity and high surface area for infiltrated nano-sized Ni particles, yielding a high TPB density that facilitates fast H_2 oxidation even at moderate temperatures.

4. Conclusions

LSGM-electrolyte SOFCs with SLT supports and infiltrated nanoscale Ni anodes yielded high power density at intermediate temperatures. The combination of high power density with cost-effective ceramic processing method and SLT support makes these a promising new class of IT-SOFCs. The maximum cell power density increased with increasing porosity, up to 30 wt.% PMMA pore former, and the Ni loading amount in the AFL. Maximum power densities were 1.12 W cm^{-2} at 650 °C and 0.42 W cm^{-2} at 550 °C, for the optimum AFL porosity of 26% and 15.0 vol.% Ni, conditions where both the pores and Ni in the AFL appeared to be mostly percolated.

5. Experimental Section

$Sr_{0.8}La_{0.2}TiO_{3-\alpha}$ (SLT) powder was prepared by calcining the appropriate amount of $SrCO_3$ (Alfa Aesar, Massachusetts), La_2O_3 (Alfa Aesar, Massachusetts) and TiO_2 (Alfa Aesar, Massachusetts) powders at 950 °C for 4 h. The SLT powder was mixed with 30 wt.% graphite (Timcal, Swizerland) by ball milling for 24 h in ethanol. This slurry was then dried, ground, and sieved. The resulting powder was pressed into 19 mm diameter pellets weighing ≈0.3 g. The pellets were pre-fired at 1320 °C for 4 h to burn off the graphite and achieve some structural strength.

The electrochemically active anode functional layer (AFL) colloidal solution consisting of $(La_{0.9}Sr_{0.1})_{0.98}Ga_{0.8}Mg_{0.2}O_{3-\delta}$ (LSGM) powder (Praxair, Washington), poly(95% methyl methacrylate/5% DVB) (PMMA Microspheres, Bangs Laboratories, Inc, Indiana) with mean diameter of 1.5 μm as pore former, poly(vinyl butyral) (PVB, Aldrich, Wisconsin) and ethyl cellulose (Aldrich, Wisconsin) as binders, polyethylenimine (PEI, Aldrich, Wisconsin) as dispersant and ethanol as solvent, was deposited on the SLT support. The AFLs contained 10 wt.%, 20 wt.%, 30 wt.% and 40 wt.% weight percent of PMMA pore formers, respectively. The porosity of the AFL was estimated from SEM images using a point counting stereological method. The porosity values were the average of values obtained from two SEM images per weight percent. This structure was then co-fired on the SLT support at 1100 °C for 2h. The LSGM electrolyte colloidal solution was subsequently deposited and sintered at 1400 °C for 4h to ensure a fully dense electrolyte. $La_{0.6}Sr_{0.4}Fe_{0.8}Co_{0.2}O_{3-\delta}$ (LSCF, Praxair, Washington) powder (50 wt.%) and $Ce_{0.9}Gd_{0.1}O_{1.95}$ (GDC, Nextech, Ohio) powder (50 wt.%) were mixed together and dispersed into a vehicle (V-737, Heraeus Inc., Pennsylvania) by a three-roll mill. LSCF ink was prepared in the same way. The cathode consisting of LSCF-GDC as functional layer and LSCF as current collector was screen printed on the electrolyte and sintered at 1100 °C for 2h. The active cathode surface area was 0.5 cm^2.

A 5 M $Ni(NO_3)_2$ (Fisher Chemicals, New Jersey) solution was infiltrated into the porous SLT support and LSGM functional layer. After calcining at 700 °C for 0.5 h, nanostructured NiO covered the SLT and LSGM surface homogeneously. The desired Ni amount was achieved by 4-12 infiltration cycles (50 μL $Ni(NO_3)_2$ solution each cycle). The NiO was reduced to Ni metal during SOFC operation under humidified hydrogen (3 vol.% H_2O).

The cells were sealed onto an alumina tube with Ag ink (DAD-87, Shanghai Research Institute of Synthetic Resins) using a four-probe configuration. The cathode was exposed to ambient air while the anode was fueled with humidified hydrogen (3 vol.% H_2O) at 50 sccm. All the cells were ramped up to 650 °C in H_2 and stabilized at 650 °C for 0.5 h. After testing from 650 °C to 450 °C, the cells were cooled down to room temperature in H_2 protection. Current-voltage curves and electrochemical impedance spectra (EIS) were recorded using an IM6 electrochemical workstation (ZAHNER, Germany). The frequency range for the impedance measurements was 100 mHz-100 kHz. Constant current was measured using a Keithley 2420 sourcemeter. The cell structure was examined by scanning electron microscopy (SEM, Hitachi S-4800-II and SU8030).

To investigate the compatibility of SLT and LSGM at high firing temperatures, the two powders were mixed together in equal amounts, then pressed and sintered at 1400 °C for 4h. These pellets were ground into a powder and loaded into quartz capillaries. High-resolution synchrotron-based powder x-ray diffraction (PXRD) experiments were performed at the Advanced Photon Source of Argonne National Laboratory. The wavelength λ was 0.72838 Å.

Acknowledgements

This work is financially supported by the Global Climate and Energy Project (GCEP, grant No. 51922). E.C.M. acknowledges support by the

DOE NNSA Stewardship Science Graduate Fellowship Program, grant DE-FC52–08NA28752. The authors gratefully acknowledge Dr. Gregory J. Halder for the great help with Synchrotron-based XRD at Argonne National Laboratory. The contribution of Daniel Fowler from Department of Chemistry at Northwestern University is greatly appreciated.

Note: Editorial notes were deleted after initial online publication. The content of the article has not been changed.

Received: January 27, 2014
Revised: April 30, 2014
Published online: July 14, 2014

[1] a) T. Suzuki, Z. Hasan, Y. Funahashi, T. Yamaguchi, Y. Fujishiro, M. Awano, *Science* **2009**, *325*, 852; b) T. Suzuki, T. Yamaguchi, K. Hamamoto, Y. Fujishiro, M. Awano, N. Sammes, *Energy Environ. Sci.* **2011**, *4*, 940; c) T. Suzuki, T. Yamaguchi, K. Hamamoto, H. Sumi, Y. Fujishiro, *RSC Adv.* **2011**, *1*, 911.
[2] K. Q. Huang, J. B. Goodenough, *J. Alloy. Compd.* **2000**, *303*, 454.
[3] Y. B. Lin, S. A. Barnett, *Electrochem. Solid State Lett.* **2006**, *9*, A285.
[4] T. Ishihara, H. Eto, J. W. Yan, *Int. J. Hydrog. Energy* **2011**, *36*, 1862.
[5] Z. L. Zhan, D. M. Bierschenk, J. S. Cronin, S. A. Barnett, *Energy Environ. Sci.* **2011**, *4*, 3951.
[6] X. J. Liu, X. Meng, D. Han, H. Wu, F. R. Zeng, Z. L. Zhan, *J. Power Sources* **2013**, *222*, 92.
[7] J. Drennan, V. Zelizko, D. Hay, F. T. Ciacchi, S. Rajendran, S. P. S. Badwal, *J. Mater. Chem.* **1997**, *7*, 79.
[8] J. H. Kim, H. I. Yoo, *Solid State Ionics* **2001**, *140*, 105.
[9] E. C. Miller, Z. Gao, S. A. Barnett, *Fuel Cells* **2013**, *13*, 1060.
[10] The following prices are presented for illustration only: $511 for 1 kg Gallium; $13.6 for 1 kg Titanium sponge metal from U.S. Geological Survey, Mineral Commodity Summaries, February 2014. Cost comparison between Gallium and Titanium is only presented, which is the main economic difference between SLT and LSGM.
[11] M. R. Pillai, Y. Jiang, N. Mansourian, I. Kim, D. M. Bierschenk, H. Y. Zhu, R. J. Kee, S. A. Barnett, *Electrochem. Solid State Lett.* **2008**, *11*, B174.
[12] a) S. Hashimoto, L. Kindermann, P. H. Larsen, F. W. Poulsen, M. Mogensen, *J. Electroceram.* **2006**, *16*, 103; b) S. Hashimoto, L. Kindermann, F. W. Poulsen, M. Mogensen, *J. Alloy. Compd.* **2005**, *397*, 245; c) T. Ishihara, Ed. *Perovskite Oxide for Solid Oxide Fuel Cells.*, Springer, Germany, **2009**; d) O. A. Marina, N. L. Canfield, J. W. Stevenson, *Solid State Ionics* **2002**, *149*, 21.
[13] M. R. Pillai, I. Kim, D. M. Bierschenk, S. A. Barnett, *J. Power Sources* **2008**, *185*, 1086.
[14] a) K. Q. Huang, J. H. Wan, J. B. Goodenough, *J. Electrochem. Soc.* **2001**, *148*, A788; b) J. M. Haag, D. M. Bierschenk, S. A. Barnett, K. R. Poeppelmeier, *Solid State Ionics* **2012**, *212*, 1.
[15] Z. L. Zhan, D. Han, T. Z. Wu, X. F. Ye, S. R. Wang, T. L. Wen, S. M. Cho, S. A. Barnett, *RSC Adv.* **2012**, *2*, 4075.
[16] X. J. Liu, X. Meng, D. Han, H. Wu, F. R. Zeng, Z. L. Zhan, *J. Power Sources* **2013**, *222*, 92.
[17] D. M. Bierschenk, M. R. Pillai, Y. Lin, S. A. Barnett, *Fuel Cells* **2010**, *10*, 1129.
[18] T. Klemenso, K. Thyden, M. Chen, H. J. Wang, *J. Power Sources* **2010**, *195*, 7295.
[19] B. D. Madsen, S. A. Barnett, *J. Electrochem. Soc.* **2007**, *154*, B501.
[20] D. Han, X. J. Liu, F. R. Zeng, J. Q. Qian, T. Z. Wu, Z. L. Zhan, *Sci. Rep.* **2012**, *2*, 462.
[21] J. M. Vohs, R. J. Gorte, *Adv. Mater.* **2009**, *21*, 943.
[22] D. W. Dees, T. D. Claar, T. E. Easler, D. C. Fee, F. C. Mrazek, *J. Electrochem. Soc.* **1987**, *134*, 2141.
[23] R. M. C. Clemmer, S. F. Corbin, *Solid State Ionics* **2004**, *166*, 251.
[24] A. N. Busawon, D. Sarantaridis, A. Atkinson, *Electrochem. Solid State Lett.* **2008**, *11*, B186.
[25] A. Torabi, A. R. Hanifi, T. H. Etsell, P. Sarkar, *J. Electrochem. Soc.* **2012**, *159*, B201.